promoting access to White Rose research papers

White Rose
Research Online

Universities of Leeds, Sheffield and York
http://eprints.whiterose.ac.uk/

This is the published version of an article in **Physical Review A - Atomic, Molecular, and Optical Physics**

White Rose Research Online URL for this paper:

http://eprints.whiterose.ac.uk/id/eprint/78435

Published article:

Freeman, JR, Maysonnave, J, Khanna, S, Linfield, EH, Davies, AG, Dhillon, SS and Tignon, J (2013) *Laser-seeding dynamics with few-cycle pulses: Maxwell-Bloch finite-difference time-domain simulations of terahertz quantum cascade lasers.* Physical Review A - Atomic, Molecular, and Optical Physics, 87 (6). 063817. ISSN 1050-2947

http://link.aps.org/doi/10.1103/PhysRevA.87.063817

White Rose Research Online
eprints@whiterose.ac.uk

PHYSICAL REVIEW A **87**, 063817 (2013)

Laser-seeding dynamics with few-cycle pulses: Maxwell-Bloch finite-difference time-domain simulations of terahertz quantum cascade lasers

Joshua R. Freeman,[1,*] Jean Maysonnave,[1] Suraj Khanna,[2] Edmund H. Linfield,[2] A. Giles Davies,[2]
Sukhdeep S. Dhillon,[1] and Jérôme Tignon[1]
[1]*Laboratoire Pierre Aigrain, Ecole Normale Supérieure, CNRS (UMR 8551), Université Pierre et Marie Curie, Université D. Diderot, 75231 Paris Cedex 05, France*
[2]*School of Electronic and Electrical Engineering, University of Leeds, Woodhouse Lane, Leeds LS9 2JT, United Kingdom*

(Received 8 March 2013; published 12 June 2013)

We implement a Maxwell-Bloch simulation for a two-level system within the finite-difference time-domain method to simulate the seeding of lasers by broadband pulse injection. The model does not make the slowly varying envelope approximation, and the full electromagnetic field is simulated so that we are able to obtain time-resolved seeding by few-cycle pulses. The model is compared to recent results on seeding of THz quantum cascade lasers to aid in the interpretation of their complex signals. The simulations are found to be in good agreement with the data when gain recovery times of 15 ps are used. Furthermore, we find that the emission from the laser depends only weakly on the seed used to initiate laser action. The model is readily applicable to any seeded laser system where few-cycle seed pulses are used.

DOI: 10.1103/PhysRevA.87.063817 PACS number(s): 42.55.Px

I. INTRODUCTION

Optical injection seeding is widely used to imprint some desirable characteristic of one "seed" laser onto another laser. The desirable characteristic is most often frequency stability; by using a seed laser with a stable frequency, it is possible to reduce the mode partition noise in modulated diode lasers [1] and produce narrowband pulses from Q-switched pulsed lasers [2,3].

The use of laser seeding, however, is not limited to frequency stabilization. We have recently made use of optical injection seeding to stabilize the phase of a laser [4]. The stabilized laser was a quantum cascade laser (QCL) operating in the terahertz (THz) region of the electromagnetic spectrum [5] and the seed was a broadband single-cycle pulse generated by a biased photoconductive antenna illuminated by a mode-locked Ti:sapphire laser. In doing this, we are making use of the fact that the pulse length of the femtosecond pulse, less than 100 fs, is significantly shorter than the period of the terahertz radiation produced by the QCL. Each femtosecond pulse is split, with one portion used to generate a single-cycle THz pulse by the use of a photoconductive antenna. The single-cycle pulse is then injected into the QCL cavity at the same moment that the QCL is brought above threshold. In this way, the THz QCL emission is initiated by the single-cycle THz pulse rather than the spontaneous emission. By seeding the laser emission in this way, the phase of the QCL emission is dictated by the femtosecond pulse. Thus, we are making use of the well-defined *temporal* aspect of the femtosecond seed pulse rather than conventional seeding, where it is the well-defined *frequency* aspect that is used. With the phase of the QCL emission stabilized to the femtosecond pulse, we are able to use the other portion of the split femtosecond pulse to sample coherently the THz field in an electro-optic crystal. It is interesting to note that while optical injection has not been used to stabilize the frequency emission of a QCL, an *electrical* feedback technique has been used to stabilize the QCL emission frequency [6].

The prospect of coherent detection of laser radiation could find technological applications because both time-domain and spectral information are available in the same measurement. In addition, this radiation falls in the traditionally underexploited THz region of the electromagnetic spectrum [7]. Besides the technological interest of this measurement, it also provides a means to study laser emission in unprecedented detail and gain insight into the operation of QCLs. The type of signals observed from seeded QCLs can vary significantly from quasiconstant [4] to a single pulse per round trip [8] and multiple pulses per round trip [9]. This variety and complexity of signals hints at the dynamics of QCLs. The important lifetimes for QCLs, namely the gain recovery time, T_1, the dephasing time, T_2, and the photon lifetime, T_{ph}, are all of the order of 1–50 ps and the cavity round-trip time is typically the same as or longer than these times, leading to complex dynamics [10].

The ultrafast dynamics of QCLs has become of particular interest recently due to progress in mode-locking of QCLs both in the mid-IR [11] and THz [12,13] regions of the spectrum. The role of the laser dynamics, particularly the gain recovery time, T_1, is a critical parameter for stable mode-locking and should also strongly affect the temporal output of seeded QCLs. Despite the importance of this parameter, there has been only one attempt to measure this parameter in THz QCLs directly [14] due to the difficulty of the measurement.

To gain a deeper understanding of the processes involved in this type of seeding by single-cycle pulses and to understand the complex signals observed, we have carried out numerical time-domain simulations using the Maxwell-Bloch formalism. These simulations help explain the role and the effect of the gain recovery time on the coherent field we observe. In addition, we are able to assess how changing the optical seed affects the emission from the laser.

II. MODEL

Previous numerical studies of dynamics in quantum cascade lasers have made use of the two-level Maxwell-Bloch

---

[*] joshua.freeman@lpa.ens.fr; j.r.freeman@leeds.ac.uk

©2013 American Physical Society

equations within the slowly varying envelope approximation. These methods have successfully described the dynamics of QCLs and have been used to model coherent instabilities [15], self-induced transparency mode-locking [16], and most recently, active mode-locking [17]. For the present work, we again make use of the Maxwell-Bloch equations. However, rather than make the slowly varying envelope approximation, we follow the method of Ziolkowski *et al.* [18] to solve the equations using the finite-difference time-domain (FDTD) method. In doing so, we directly compute the *electric field* rather than the envelope of the field. This is particularly important in our case because the seed pulse is single-cycle and therefore cannot be approximated by a slowly varying envelope. A similar method was used by Darmo *et al.* [19] to understand the interaction of a THz pulse with a two-level gain medium, but the laser dynamics was not investigated.

The system being investigated is ideal to simulate because the experiment and simulation are conceptually identical. In the experiment, the sample is prepared in a nonequilibrium state before the seed pulse arrives, ensuring that there is no laser emission in the cavity before the seed pulse arrives and any emission is initiated by the seed pulse. The output from the sample can then be measured coherently as a function of time for the first few nanoseconds of the emission. The simulation is done in the same way: at $t = 0$, a seed pulse is injected into the cavity, containing a population inversion, and the output is monitored over time, as shown schematically in Fig. 1.

We follow the formulation of Ref. [17] and describe the QCL gain region as an open two-level system with an upper level (2) and a lower level (1), with the latter always empty. For that case, the Bloch equations are

$$\partial_t \rho_{12} = -\left(\frac{1}{T_2} - j\omega_{12}\right)\rho_{12} + \frac{E_x M}{j\hbar} w - \frac{2E_x X}{j\hbar}\rho_{12}, \tag{1}$$

$$\partial_t w = \frac{2E_x M}{j\hbar}(\rho_{12}^* - \rho_{12}) - \frac{w - w_0}{T_1}. \tag{2}$$

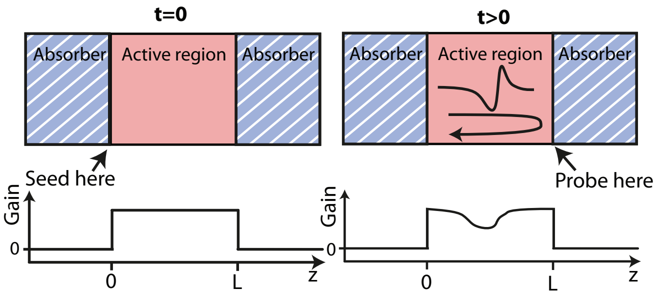

FIG. 1. (Color online) Schematic of the simulation. The active region has a relative permittivity of $\epsilon_r = 12.9$, a waveguide loss of 3 cm^{-1}, and an unsaturated gain of 21 cm^{-1}. The absorber regions have a relative permittivity of $\epsilon_r = 1$, a loss of 3×10^4 cm^{-1}, and zero gain. The seed is launched at $t = 0$ on the left facet and the signal is probed just outside the right facet.

Here, ρ_1 and ρ_2 are the fractional populations of states 1 and 2, $\rho_{12} = \rho_{21}^*$ represents the coherence between the two states, and $w = \rho_2 - \rho_1$ is the population inversion between the two states. The energy of the transition between the two levels is $\hbar\omega_{12}$, $M = e\langle 2|x|1\rangle$ is the dipole matrix element, and E_x is the electric field coupling to the transition. The value of the population inversion without the presence of radiation is w_0 and the characteristic lifetime for the return to this value is T_1, the gain recovery time. The dephasing time for the transition is given by T_2. We have also included a term in Eq. (1) that is usually ignored:

$$X = \frac{e}{2}\left(\langle 2|x|2\rangle - \langle 1|x|1\rangle\right). \tag{3}$$

For atomic systems this term will clearly be zero as the wave functions of the two states are centered around the same point in space. However, for our case of intersubband transitions in a superlattice under an applied bias, the value of X will be nonzero. We have performed simulations with realistic values of this parameter ($X = 16$ nm for the active region under investigation) and found that the effect on the resulting signal is very small. Therefore, for the remainder of this work we shall ignore this term. It should be noted, however, that for some active regions with highly diagonal transitions (e.g., [20]) this factor may become important. Another point to note is that rather than follow Ref. [17] and parametrize the last term of Eq. (2) with a pumping parameter, $J \propto \lambda = \frac{w_0}{T_1}$, proportional to the injection current, we prefer to use the unclamped population inversion as we have a reliable measurement of the unclamped gain in our devices [21].

To obtain real equations for computation and agreement with the notation of Ziolkowski *et al.* [18], we make the substitution $2\rho_{12} = \rho_a - j\rho_b$ and, by recalling that the polarization of the medium is $P_x = -2NM\rho_a$ (N is the number of identical two-level systems), we link the Maxwell and Bloch equations to obtain the set of real equations:

$$\partial_t H_y = -\frac{1}{\mu_0}\frac{\partial E_x}{\partial z}, \tag{4}$$

$$\partial_t E_x = -\frac{1}{\varepsilon}\frac{\partial H_y}{\partial z} - \frac{NM}{\varepsilon T_2}\rho_a + \frac{NM\omega_{21}}{\varepsilon}\rho_b - lE_x, \tag{5}$$

$$\partial_t \rho_a = -\frac{1}{T_2}\rho_a + \omega_{12}\rho_b, \tag{6}$$

$$\partial_t \rho_b = -\frac{1}{T_2}\rho_b - \omega_{12}\rho_a + \frac{2E_x M}{\hbar} w, \tag{7}$$

$$\partial_t w = -\frac{w - w_0}{T_1} - \frac{2E_x M}{\hbar}\rho_b. \tag{8}$$

Here we have also added at term, $(-lE_x)$, to account for the waveguide loss. This set of equations is then solved using the FDTD predictor-corrector method proposed by Ref. [18]. We do not analytically factor out the decay terms T_1 and T_2 because this is only possible for a single-pass model [18]; we do not find that this introduces problems of numerical stability.

III. SAMPLE

Equations (4)–(8) will propagate an electromagnetic field traveling in the z direction through a homogeneous medium containing N two-level systems per unit volume [22]. The Fabry-Pérot cavity of the active region is formed by imposing a refractive index of $\epsilon_r = 1$ outside the active region, indicated in Fig. 1. This leads to a reflection of around 30% at the boundary, in good agreement with other studies and experiments [23–25]. The region outside the cavity is made highly lossy to

TABLE I. Parameters used in the simulations.

Symbol	Name	Value(s)
ε_r	Background relative permittivity	12.9
T_1	Gain recovery time	5–50 ps
T_2	Dephasing time	2.35 ps
w_0	Equilibrium population inversion	1
N	Number of oscillators	3.7×10^{20} m^{-3}
M/e	Dipole matrix element	6.2 nm
ω_{12}	Transition frequency	$2\pi \times 2.45$ THz
l	Waveguide loss	3 cm^{-1}
L	Cavity length	1.5 and 3 mm

ensure that reflections from the fixed boundary conditions are suppressed.

The seed pulse is launched into the cavity by modulating the value of the electric field on the left facet. However, the field value on this facet must be allowed to vary freely before the seed returns. This places an upper bound on the duration of the seed pulse, which is the cavity round-trip time. In our case, the seed easily fulfills this criterion. We approximate the seed pulse generated by the photoconductive antenna as a single cycle pulse with a characteristic width of 0.35 ps, which we measure experimentally. We also observe an echo in the seed pulse experimentally, around 36 ps after the main pulse, due to the finite thickness of the photoconductive antenna, and we have included this effect in the seed.

The active region that we have chosen to simulate is a bound-to-continuum design [26], with the active region modified to emit at 2.45 THz. The active region was selected because it was also used in Ref. [21], where the maximum unclamped gain was measured to be 21 cm^{-1}. We have used this value to choose the value of N, shown in Table I, together with the other parameters required by the numerical simulation. The values of ω_{12} and T_2 were found from the center frequency and bandwidth of the laser spectra, and the value of w_0 was chosen to be 1 for the peak value of the gain. The value of M was calculated from the band structure of the active region.

The loss for the waveguide was found by comparing the value of the clamped gain from measurements when the laser is operating and the gain clamped [25]. We find a waveguide loss of $\alpha_w = 3$ cm^{-1} after accounting for the mirror losses. Therefore, the only parameter that is not well known is T_1, the gain recovery time. In the following simulations, we use values of T_1 between 5 and 50 ps and we study the dependence of the simulation on this value. A space step size of $dz = \lambda/150$ and a time step of $dt = dz/c_0$ were used for the FDTD simulations.

For the cavity length, L, we will compare two commonly used cavity lengths: 1.5 and 3 mm. The cavity length is an easy parameter to change experimentally and can provide insight into the laser dynamics because it changes the ratio between the cavity round-trip time and the gain recovery time. The cavity round-trip times for 1.5 and 3 mm cavities are 36 and 72 ps, respectively. Changing the cavity length also changes the photon lifetime in the cavity, estimated to be 11 and 17 ps, respectively, for the 1.5 and 3 mm cavity. In terms of loss, the total loss will be 11 and 7 cm^{-1}, respectively, for the 1.5 and 3 mm cavity. Also, given the smaller free spectral range of the longer Fabry-Pérot cavity, there will be more modes present in the longer cavity.

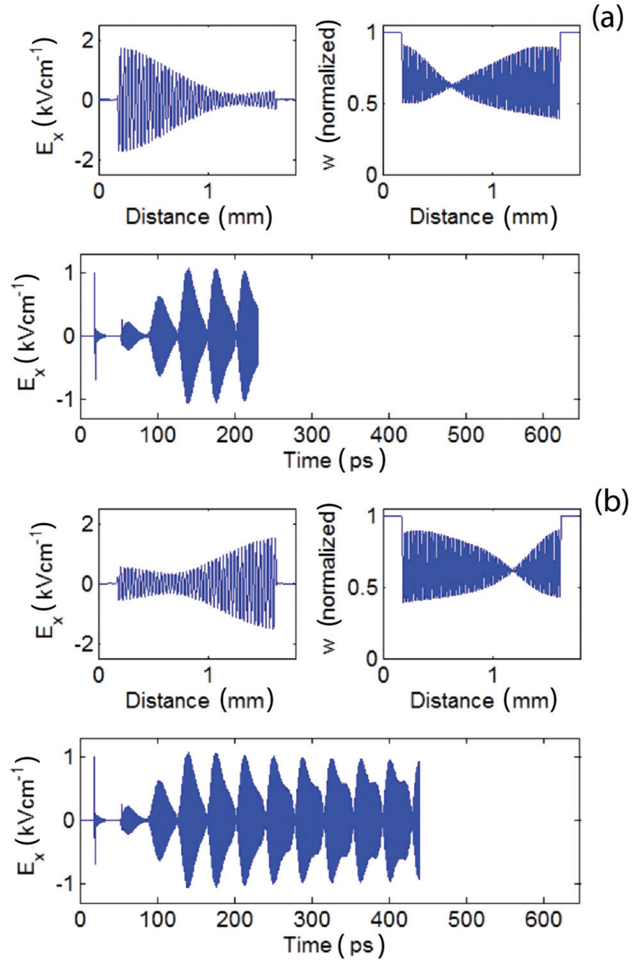

FIG. 2. (Color online) Stills from a video of a simulation for a 1.5 mm cavity using a gain recovery time of 20 ps, showing the simulation after (a) 230 ps and (b) 440 ps. The video is available in the Supplemental Material.

It is interesting to compare the value of N found above to the number of carriers present in the sample through doping. The average nominal doping in the active region is 0.37×10^{22} m^{-3}. By taking into account the number of periods (90) and the overlap of the optical mode with the active region (~30%), we find a maximum possible number of active carriers of 7.8×10^{22} m^{-3}. Comparing this with the value of N in Table I implies a conversion efficiency of 0.5%, in good agreement with the 0.5–5 % commonly measured for this type of design by more conventional methods [27,28].

IV. RESULTS

Figure 2 shows the results from a typical simulation with $L = 1.5$ mm and $T_1 = 20$ ps. A full video of the seed pulse evolution is included in the Supplemental Material [33]. We see that the seed pulse is quickly amplified and forms a standing wave in the cavity. This standing wave induces spatial hole burning (SHB) in the gain medium, seen as a rapid variation of the population inversion, w, over the length of the cavity. In some lasers (diode lasers are an important example), lateral

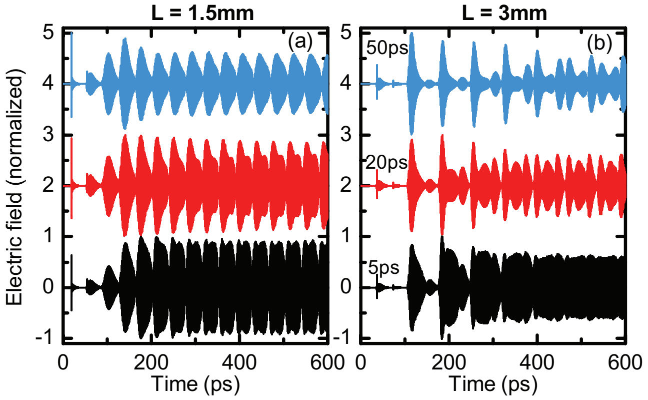

FIG. 3. (Color online) Numerical simulations for (a) 1.5 mm and (b) 3 mm cavities using gain recovery times of $T_1 = 5$, 20, and 50 ps. The simulations are normalized and offset for clarity.

electron diffusion counteracts the effect of SHB. However, this effect is thought to be weak in QCLs [15,17] and the model assumes that there is no lateral electron diffusion.

It is also interesting to note that the node in the SHB of the population inversion does not occur at the same position as the minimum of the intracavity electric field. This is because the electric field, E_x, and the population inversion, w, are connected through the polarization, causing the population inversion to lag the electric field.

From the simulation we record the emission from the laser cavity at the opposite facet to the injection (as in the experimental measurements) and we plot the electric field emission from the laser cavity over time. We show this in Fig. 3 for 1.5 and 3 mm cavities and $T_1 = 5$, 20, and 50 ps.

The differences between the two cavity lengths are quite marked. The simulated signals from the shorter, 1.5 mm cavity shows essentially one pulse for each cavity round trip, while the longer 3 mm cavity shows signals that are more complex, with two or three pulses distinguishable for each cavity round trip. One reason for more complex pulse formation is the larger number of modes operating above threshold, leading to more intermode beating. As the gain recovery time, T_1, is decreased from 50 to 5 ps, it is noticeable how the emission intensity tends to become more continuous. This is because the faster gain recovery allows amplification even a short time after a pulse has passed.

We can now make a closer comparison between these simulations and the data that we typically measure for this active region, shown in Fig. 4. The data have been acquired from two samples with lengths of 1.5 and 3 mm. The experimental setup is the same as that in Refs. [4] and [9], and the details can be found in those articles.

The simulations that give the best agreement with the data use a gain recovery time of 15 ps, and these are also shown in Fig. 4 for comparison. We see that there is good qualitative agreement between the simulations and experiment for both cavity lengths under investigation, particularly given the variety of seeded signals that can be generated. For the 1.5 mm cavity, the numerical simulation reproduces several features of the data, including one pulse per round trip and an asymmetric pulse shape. The asymmetric pulse shape appears to originate from the amplification of the seed pulse on the first pass in the cavity. For the 3 mm cavity, the emission is much more complex, however the essential features of the data are captured in the simulation; both show three identifiable pulses per round trip and a null in the field in each round trip.

The value of 15 ps for the gain recovery time is less than that found by Green *et al.* [14] of 50 ps for a similar THz QCL design, but larger than the values measured for mid-IR QCLs of 2–3 ps [29]. Another relevant work by Scalari *et al.* [30] found

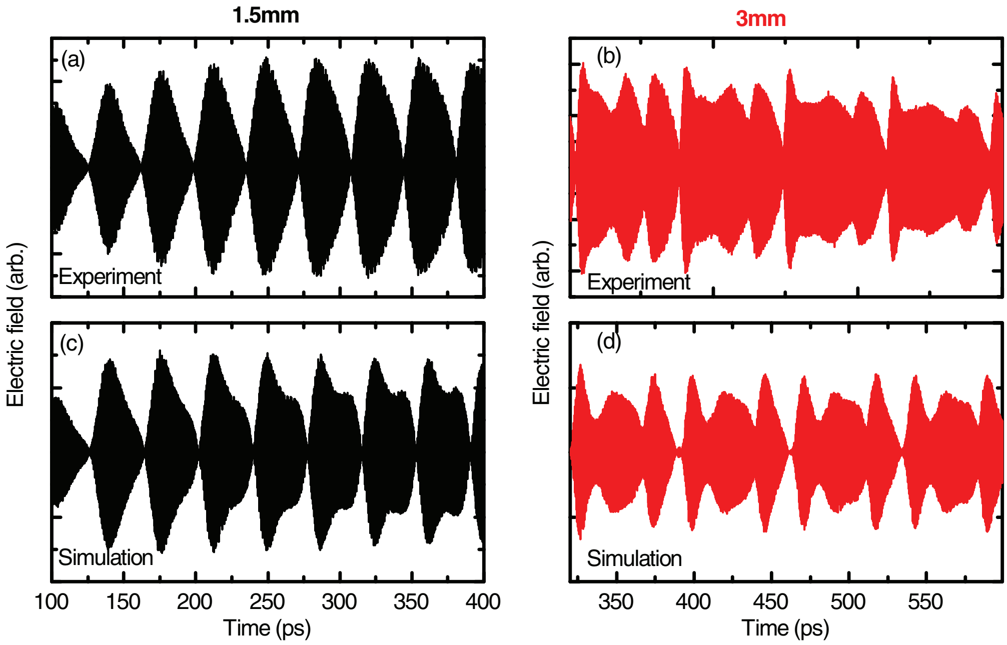

FIG. 4. (Color online) A comparison between experimental data and simulation for 1.5 and 3 mm cavities. Parts (a) and (b) show experimental data for 1.5 and 3 mm cavities, respectively. Parts (c) and (d) show the corresponding simulations. The value of gain recovery time used in these simulations is 15 ps.

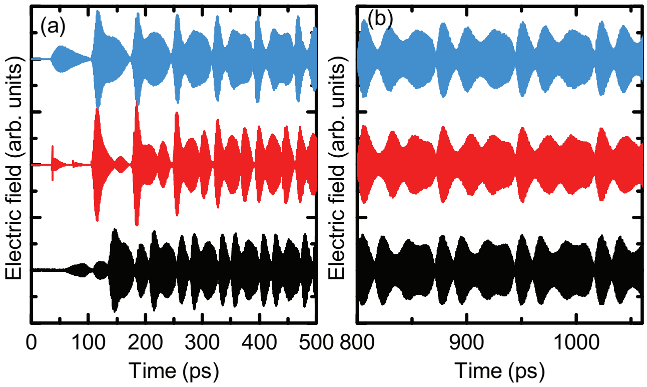

FIG. 5. (Color online) A comparison of different seed pulses for a 3 mm cavity. Blue (upper): The cavity is seeded by a narrow-band pulse resonant with the laser transition and is 50 ps long. Red (middle): A short seed pulse, as in Fig. 4. Black (lower): A random perturbation is made to the cavity and evolves. (a) The first 500 ps after the seed arrives. (b) Simulation after 1 ns. In this figure, the time delay of each trace has been shifted to facilitate comparison.

an upper state lifetime for a THz QCL of 12 ps [31], much closer to the value we deduce here. The measurement of Green *et al.* might best be described as the system recovery time because the quantity measured in the pump-probe experiment was the photocurrent through the entire structure. Thus it may overestimate the microscopic gain recovery time that we use in our model.

We can also use this simulation to understand the dependence of the laser output on the seed pulse by changing the type of optical seed that we inject; Fig. 5 shows the results of these comparisons. We investigated two cases in addition to the experimental situation of an ultrashort pulse with a broad spectrum: (i) A narrowband pulse at the QCL frequency (Fig. 5, blue) and (ii) random noise (Fig. 5, black). The narrowband pulse, with a frequency of 2.45 THz and a duration of 50 ps, was chosen as a contrast to the single cycle seed pulse. The random seed represents an approximation of how the laser would start naturally (on spontaneous emission), a regime that we are unable to access experimentally due to the synchronization requirements of the measurement [9]. The random seed was approximated by introducing a random electric field perturbation along the entire length of the cavity at $t = 0$ and letting the emission evolve freely.

For each of these different seeds, we find that the resulting emission is remarkably similar after a few cavity round trips (∼1 ns); see Fig. 5(b). This finding suggests that the exact form of the seed does not greatly affect the emission produced by the laser, and therefore the electric field that we measure experimentally from the laser is very similar to the emission from a free-running laser.

We have also investigated the effect of changing the seed amplitude on the QCL emission. While we do not see any change in the form of the emission at longer times, we do find that the "buildup" time is longer for weaker seed pulses.

V. CONCLUSIONS

We have developed a numerical simulation to describe the seeding of a laser by few-cycle broadband pulses by using a model based on Maxwell-Bloch equations solved under the FDTD framework. This model has been applied to the seeding of THz QCLs with single-cycle THz pulses and compared with the experimental results. The simulations are in good agreement with the experimental data, reproducing the differing signals observed for different cavity lengths. The least well known parameter in the model is the gain recovery time, T_1. However, we see good qualitative agreement with the data when using a value of 15 ps, which compares favorably with the value previously found in Ref. [30]. This value, shorter than the round-trip time, suggests that commonly employed mode-locking techniques where the laser is continuously pumped will not be possible as the gain medium cannot store sufficient energy. However, synchronous pumping [32] techniques are possible routes to mode-locking [12,13].

The dependence of the electric field emission on the seed pulse was also examined. It was found that electric field emission from the QCL laser is largely insensitive to the type of seed used, implying that the experimentally observed signals closely resemble the "natural" emission of the QCL. This is somewhat counter to the more established idea of seeding that is conventionally used to fix the frequency of the laser to a seed laser.

ACKNOWLEDGMENTS

We are grateful for support from the "Agence Nationale de la Recherche" (ANR, Contract No. HI-TEQ ANR-09-NANO-017), the EPSRC (UK), the ERC programmes NOTES and TOSCA, and to the Royal Society and Wolfson Foundation. J.R.F. acknowledges funding from a Marie Curie fellowship (Grant No. 274602).

---

[1] K. Iwashita and K. Nakagawa, IEEE J. Quantum Electron. **18**, 1669 (1982).
[2] J. Yu, U. N. Singh, N. P. Barnes, and M. Petros, Opt. Lett. **23**, 780 (1998).
[3] S. Hannemann, E.-J. van Duijn, and W. Ubachs, Rev. Sci. Instrum. **78**, 103102 (2007).
[4] D. Oustinov, N. Jukam, R. Rungsawang, J. Madeo, S. Barbieri, P. Filloux, C. Sirtori, X. Marcadet, J. Tignon, and S. Dhillon, Nat. Commun. **1**, 69 (2010).
[5] B. S. Williams, Nat. Photon. **1**, 517 (2007).
[6] S. Barbieri, P. Gellie, G. Santarelli, L. Ding, W. Maineult, C. Sirtori, R. Colombelli, H. Beere, and D. Ritchie, Nat. Photon. **4**, 636 (2010).
[7] Y.-S. Lee, *Principles of Terahertz Science and Technology* (Springer, New York, 2009) .
[8] J. Maysonnave, K. Maussang, J. R. Freeman, N. Jukam, J. Madéo, P. Cavalié, R. Rungsawang, S. Khanna, E. Linfield, A. Davies, H. Beere, D. Ritchie, S. Dhillon, and J. Tignon, Opt. Express **20**, 20855 (2012).

[9] J. Maysonnave, N. Jukam, M. S. M. Ibrahim, R. Rungsawang, K. Maussang, J. Madéo, P. Cavalié, P. Dean, S. P. Khanna, D. P. Steenson, E. H. Linfield, A. G. Davies, S. S. Dhillon, and J. Tignon, Opt. Express **20**, 16662 (2012).

[10] G. H. van Tartwijk and G. P Agrawal, Prog. Quantum Electron. **22**, 43 (1998).

[11] C. Y. Wang, L. Kuznetsova, V. M. Gkortsas, L. Diehl, F. X. Kartner, M. A. Belkin, A. Belyanin, X. Li, D. Ham, H. Schneider, P. Grant, C. Y. Song, S. Haffouz, Z. R. Wasilewski, H. Liu, and F. Capasso, Opt. Express **17**, 12929 (2009).

[12] S. Barbieri, M. Ravaro, P. Gellie, G. Santarelli, C. Manquest, C. Sirtori, S. P. Khanna, E. H. Linfield, and A. G. Davies, Nat. Photon. **5**, 306 (2011).

[13] J. R. Freeman, J. Maysonnave, N. Jukam, P. Cavalie, K. Maussang, H. E. Beere, D. A. Ritchie, J. Mangeney, S. S. Dhillon, and J. Tignon, Appl. Phys. Lett. **101**, 181115 (2012).

[14] R. P. Green, A. Tredicucci, N. Q. Vinh, B. Murdin, C. Pidgeon, H. E. Beere, and D. A. Ritchie, Phys. Rev. B **80**, 075303 (2009).

[15] A. Gordon, C. Y. Wang, L. Diehl, F. X. Kärtner, A. Belyanin, D. Bour, S. Corzine, G. Höfler, H. C. Liu, H. Schneider, T. Maier, M. Troccoli, J. Faist, and F. Capasso, Phys. Rev. A **77**, 053804 (2008).

[16] C. R. Menyuk and M. A. Talukder, Phys. Rev. Lett. **102**, 023903 (2009).

[17] V.-M. Gkortsas, C. Wang, L. Kuznetsova, L. Diehl, A. Gordon, C. Jirauschek, M. A. Belkin, A. Belyanin, F. Capasso, and F. X. Kärtner, Opt. Express **18**, 13616 (2010).

[18] R. W. Ziolkowski, J. M. Arnold, and D. M. Gogny, Phys. Rev. A **52**, 3082 (1995).

[19] J. Darmo, J. Kroll, and K. Unterrainer, in *Theoretical Aspects of Time-domain Spectroscopy of Semiconductor Terahertz Gain Medium*, AIP Conf. Proc. No. 893 (AIP, New York, 2007), p. 515.

[20] S. Kumar, Q. Hu, and J. L. Reno, Appl. Phys. Lett. **94**, 131105 (2009).

[21] N. Jukam, S. S. Dhillon, D. Oustinov, J. Madeo, C. Manquest, S. Barbieri, C. Sirtori, S. P. Khanna, E. H. Linfield, A. G. Davies, and J. Tignon, Nat. Photon. **3**, 715 (2009).

[22] We only consider one component of the electric field in this case because only transitions coupling to an electric field in the growth direction (x direction in this model) are allowed by the intersubband selection rules.

[23] C. M. Herzinger, C. C. Lu, T. A. DeTemple, and W. C. Chew, IEEE J. Quantum Electron. **29**, 2273 (1993).

[24] S. Kohen, B. S. Williams, and Q. Hu, J. Appl. Phys. **97**, 053106 (2005).

[25] N. Jukam, S. Dhillon, Z.-Y. Zhao, G. Duerr, J. Armijo, N. Sirmons, S. Hameau, S. Barbieri, P. Filloux, C. Sirtori, X. Marcadet, and J. Tignon, IEEE J. Sel. Top. Quantum Electron. **14**, 436 (2008).

[26] S. Barbieri, J. Alton, H. E. Beere, J. Fowler, E. H. Linfield, and D. A. Ritchie, Appl. Phys. Lett. **85**, 1674 (2004).

[27] J. R. Freeman, O. P. Marshall, H. E. Beere, and D. A. Ritchie, Appl. Phys. Lett. **93**, 191119 (2008).

[28] M. S. Vitiello, G. Scamarcio, V. Spagnolo, S. S. Dhillon, and C. Sirtori, Appl. Phys. Lett. **90**, 191115 (2007).

[29] H. Choi, T. B. Norris, T. Gresch, M. Giovannini, J. Faist, L. Diehl, and F. Capasso, Appl. Phys. Lett. **92**, 122114 (2008).

[30] G. Scalari, R. Terazzi, M. Giovannini, N. Hoyler, and J. Faist, Appl. Phys. Lett. **91**, 032103 (2007).

[31] The upper state lifetime and gain recovery time are equivalent in this two-level model.

[32] A. E. Siegman, *Lasers* (University Science Books, Mill Valley, CA, 1989).

[33] See Supplemental Material at http://link.aps.org/supplemental/10.1103/PhysRevA.87.063817 for a full video of the seed pulse evolution.